Effect of Gd and Sr Ordering in A Sites of Doped $Gd_{0.2}Sr_{0.8}CoO_{3-\delta}$ Perovskite on Its Structural, Magnetic, and Thermodynamic Properties.

V.A. Dudnikov[1], Yu.S. Orlov[1,2], S.Yu. Gavrilkin[3], M.V. Gorev[1], S.N. Vereshchagin[4], L.A. Solovyov[4], N.S. Perov[5], S.G.Ovchinnikov[1,2]

[1]*Kirensky Institute of Physics, 660036, Krasnoyarsk, Russia*

[2]*Siberian Federal University, Krasnoyarsk, 660041, Russia*

[3]*Lebedev Physical Institute, 119991, Moscow, Russia*

[4]*Institute of Chemistry and Chemical Technology, 660036, Krasnoyarsk, Russia*

[5]*Lomonosov Moscow State University, faculty of physics, 119991, Moscow, Russia*

Corresponding Author Details: Yu. S. Orlov, Kirensky Institute of Physics, 660036, Krasnoyarsk, Russia, Tel: +7(391) 243-26-35, Fax: +7(391) 243-89-23, Email: orlov@iph.krasn.ru

Abstract

Magnetic and thermodynamic properties of perovskite $Gd_{0.2}Sr_{0.8}CoO_{3-\delta,}$ with ordered and disordered states of *Gd* and *Sr* in the *A*-sites of the crystal lattice have been studied revealing remarkable differences in the physical properties of the ordered and disordered states. The ordered samples have larger oxygen non-stoichiometry, heat capacity and thermal expansion anomalies, and abnormal temperature dependence of the magnetization around 350 K.

Keywords: substituted rare earth cobalt oxides, magnetic and thermodynamic properties, thermoelectric oxide materials, ordered and disordered states.

I. Introduction

Substituted rare-earth perovskites $Re_{1-x}M_xCoO_{3-\delta}$ (where *Re* is the rare-earth element, and *M* is the alkaline-earth metal) belong to the large class of compounds with strong electron correlations (SEC) where complicated interplay of spin, charge, orbital, and lattice degrees of freedom takes place.[1-3] Physical and chemical properties of these compounds strongly depend on the composition and the doping level *x*[4-9], as well as on the oxygen concentration. The estimation of the oxygen non-stoichiometry has been carried out in several publications[10-12], and its effect on the cobaltate properties has been studied by several groups.[13-18] A variable magnetic state stability in cobaltates depends not only on the degree of oxygen non-stoichiometry; the ordering of cations in the *A*-sites also has an important impact. The uncontrolled state of cationic distribution may be the reason of rather large discrepancies in the magnetic susceptibility of the $Re_{1-x}M_xCoO_{3-\delta}$ reported by different researchers.

Knowledge of the dependence of the cobaltates properties on the substitution degree, the oxygen non-stoichiometry, and the degree of dopant atom ordering and vacancies in the crystal lattice[19-20], as well as the control of spin crossover temperature by the isovalent substitution of rare-earth ions[21], provides additional opportunities for the synthesis of materials with desired magnetic, thermoelectric and catalytic properties. For compounds $Gd_{1-x}Sr_xCoO_{3-\delta}$ ($0.5 < x < 0.9$) we have demonstrated recently[22-23] an increased catalytic activity and selectivity in the deep oxidation reaction of CH_4 due to a disordering of Sr^{2+}/Gd^{3+} ions over the *A*-sites of the crystal lattice in comparison to the ordered state. In this paper we present experimental data of the magnetic susceptibility and thermodynamic properties of $Gd_{0.2}Sr_{0.8}CoO_{3-\delta}$ with *A*-cation order/disorder, which depend on the thermal treatment. The degree of order/disorder is controlled by X-ray diffraction (XRD) crystal structure analysis.

One of the reasons of our interest on substituted cobaltates is the high thermoelectricity found in these materials. The possibility of obtaining substituted compounds with the general formula $Re_{1-x}M_xCo_{1-y}Me_yCoO_{3-\delta}$, where *Me* is the transition metal allows us varying in a wide range the Seebeck coefficient, electrical conductivity, and thermal conductivity.[24-25] It should be noted that the known data on the influence of the partial replacement of the rare earth element or cobalt cations by the cations of other metals, as well as its thermal history, is limited and in some cases contradictory. Not so long ago, it was shown that single crystals of mixed cobaltates Na_xCoO_2 have a thermoelectric figure of merit $ZT > 1$, which resulted in an active investigation of these thermoelectric materials (TM). Unfortunately, despite the fact that the compound Na_xCoO_2 has a good thermoelectric figure of merit, it has low chemical and thermal stability. For $Ca_2Co_2O_5$ samples, it was found $ZT \approx 1.2 – 2.7$ at $T \geq 873$ K[26], and for $Bi_2Sr_2Co_2O_y$ the figure of merit was $ZT \geq 1.1$ at 973 K.[27] Moreover, these compounds have a layered structure, which leads to anisotropy of their physical properties and potential technological problems.[28-29] Also close and promising TM are simple perovskite-like rare earth cobalt oxides $RCoO_3$, where *R* is a rare earth element, which showed a high Seebeck coefficient $S \approx 600$ μV/K.[30-32] Ceramic samples based on such TM are p-type semiconductors containing no toxic elements and are stable in oxidizing environments. However, even a slight change in the oxygen non-stoichiometry ($\delta < 0.002$) in $LaCoO_3$ greatly changes the temperature behavior and sign of thermoelectric power. Thus, at the present time different thermoelectric devices require further research and study of TM of different classes having optimal thermoelectric performance at different operating temperatures ranging from cryogenic temperatures (high temperature superconductor microelectronics) and ending with a temperature ~ 1200 K (for heat utilization in the space industry).

II. Sample preparation and measurements

Sample preparation

Polycrystalline ceramic samples of $Gd_{0.2}Sr_{0.8}CoO_{3-\delta}$ were prepared from a stoichiometric composition of oxides Co_3O_4 (99.7 %, metals basis), Gd_2O_3 (99.99 %, REO), and $SrCO_3$ (99.99 %, metals basis) that were carefully mixed and heated at 1473 K in a platinum crucible in air during 24 hours, with repeated regrinding/baking every 8 hours. After the annealing, the mixture was reground, and the powder was pressed to form pellets in the shape of bricks 5*10*2 мм. The pellets were annealed in air for 4 hours at 1473 K, and then slowly cooled at the speed of 0.033 K/s together with the furnace down to room temperature. XRD analysis showed that this annealing procedure gave *A*-site ordered samples denoted further as GSC-ord. Disordered samples (GSC-dis) were obtained by heating the pellets described above at 1473 K for 30 min, rapid quenching to 1000 K (ca. 50 K/s), with further cooling down to room temperature. All the samples were additionally heated 24 hours at 773 K for oxygen content stabilization and slowly (0.033 K/s) cooled down to room temperature. This procedure gave two groups of samples with different degree of Gd^{3+} and Sr^{2+} ordering in the *A*-sites of the perovskite crystal lattice.

XRD analysis

Powder XRD patterns were recorded on a PANalytical X'Pert PRO diffractometer with a solid state detector PIXcel using *Co* K_α radiation. The samples were prepared by grinding with octane in an agate mortar. High-temperature measurements were performed using an Anton Paar HTK 1200N stage. The lattice parameters were determined from the diffraction peak positions by the ITO program.[33] The crystal structure parameters were determined and refined using the full-profile Rietveld approach[34] by the derivative difference minimization (DDM) method.[35]

Thermochemical measurements

Thermochemical measurements were carried out in a Netzsch STA Jupiter 449C differential scanning calorimeter, equipped with a Aeolos QMS 403C mass spectrometer and a special sample holder for C_p measurements.

Thermogravimetric measurements (TGM) were performed under dynamic argon–oxygen atmosphere (0.05 – 20 vol. % O_2) in platinum crucibles, the sample mass taken for the experiments was 25 – 30 mg.

Oxygen content and non-stoichiometry index δ were calculated from the mass loss[36] measured by the thermogravimetric reduction, assuming that the cobalt is reduced to the metallic state (1).

$$Gd_{0.8}Sr_{0.2}CoO_{3-\delta} + ((3-\delta) - 1.4)\ H_2 = 0.4\ Gd_2O_3 + 0.2\ SrO + Co + ((3-\delta) - 1.4)\ H_2O \quad (1)$$

All experiments have been done in a stream of argon with 5% H_2, heating the samples up to 1173 K with a rate of 0.166 K/s. Al_2O_3 crucibles with percolated lid were used for the reduction process, and a sample mass is 22 $\pm$ 0.5 mg. The measurements were carried out with correction for the buoyancy force, i.e. blank experiments (base line) have been performed at the same conditions with empty crucibles. The accuracy of *δ*-value determination was ± 0.01.

Heat capacity of the samples was calculated according to equation (2) from DSC data (ASTM E 1269 method).

$$C_P = \frac{m_{st}}{m_{sa}} \frac{DSC_{sa} - DSC_{bl}}{DSC_{st} - DSC_{bl}} C_{P,st} \quad (2)$$

where $C_{P,st}$ is the tabulated specific heat of the standard at temperature T, m_{st}, m_{sa} are masses of the standard and the sample, DSC_{sa}, (DSC_{st}, DSC_{bl}) is the value of DSC signal at temperature T from the sample (the standard, the baseline) curve.

Three different runs under the same conditions (dynamic argon-oxygen atmosphere 20 vol. % O_2, the heating rate 0.166 K/s) were carried out: the baseline (empty platinum crucibles with perforated lids); a standard sapphire disk (40 mg) in the sample crucible; the sample under investigation (38 mg, pressed as a disk of 5 mm in diameter) in the sample crucible. All runs were repeated three times to ensure the reproducibility of the data.

Thermal expansion

The linear thermal expansion was measured in the temperature range 100 – 700 K with an induction dilatometer Netzsch DIL – 402C calibrated with a silica glass as a standard in dynamic mode with heating and cooling rate 0.05 K/s in a flow of dry helium (O_2 concentration is about 0.05 % of volume). The sample loading was 30 cN.

Magnetic measurements

Magnetic field and temperature dependences of magnetization in the temperature range 2 – 400 K were measured with the Physical Properties Measurement System (PPMS-9) by Quantum Design. The relative measurement error was smaller than the line width in the experimental curves of the magnetic susceptibility.

III. Discussion of results

The XRD and thermal analysis showed that the structure and chemical composition of $Gd_{0.2}Sr_{0.8}CoO_{3-\delta}$ was notably modified depending on the heating/cooling regimes. These modifications were revealed from the endo-/exo-thermal effects in the DSC curves, the mass evolution, and respective changes in the XRD patterns. Above 1473 K a cubic non-stoichiometric perovskite phase with randomly distributed *Gd/Sr* sites in the crystal lattice was detected (Fig. 1(c), 2(b)). At slow cooling (0.033 – 0.333 K/s) in the range 1263 – 1363 K an exothermic process takes place, that may be related to a phase transition from cubic to

tetragonal phase with a superstructure formation where the cations *Sr/Gd* and anionic vacancies are ordered (Fig. 1(a), 2(a)). A similar superstructure has been described previously.[37-40] A reversed transition from the ordered tetragonal phase to the disordered cubic one takes place at heating in the range 1273 – 1403 K, the maximum of the transition rate being at T_m = 1383 K (Fig. 3, insert). A rapid cooling from 1473 K with the rate 50 K/s leads to the formation of an *A*-site disordered cubic perovskite phase (Fig. 1(b), 2(b)). Thus, the obtained quenched metastable state is stabilized in air below 1073 K.

Table 1: Characteristic of the $Gd_{0.2}Sr_{0.8}CoO_{3-\delta}$ samples.

Sample	Cooling rate from 1473 K	Distribution of *Sr/Gd*	Oxygen index δ	*n*, Co^{+n}
GSC-ord	Annealed; 0.033 K/s	Ordered	0.37	+3.06
GSC-dis	Quenched; ~ 50 K/s	Disordered	0.29	+3.22

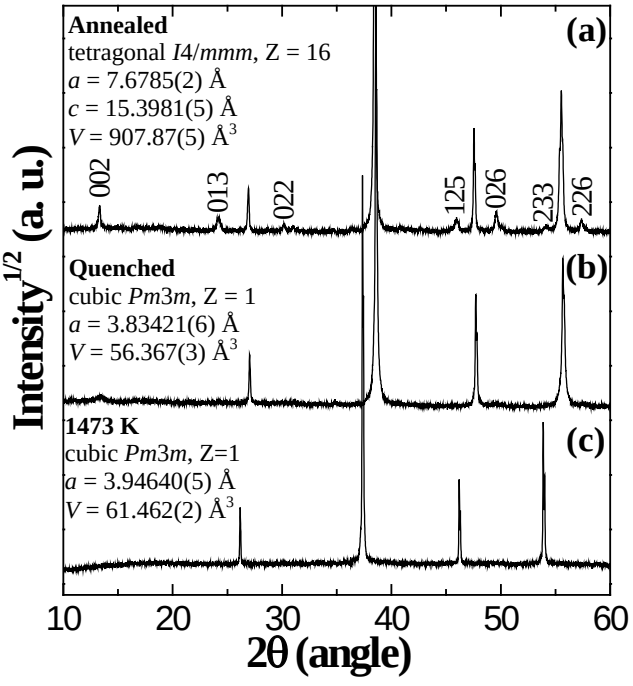

Figure 1: Fragments of XRD patterns of annealed sample GSC-ord (a), quenched sample GSC-dis (b), and sample at 1473 K (c). Tetragonal perovskite superstructure reflexions are indexed in (a). Lattice parameters and unit cell volumes are given in the inserts.

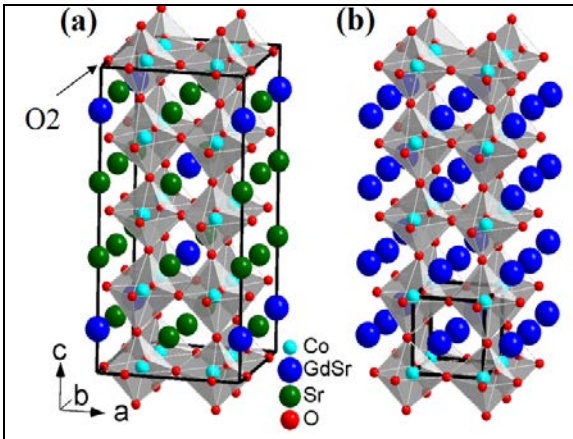

Figure 2: Crystal structures of the *A*-site ordered phase GSC-ord (a) and the disordered one GSC-dis (b) of perovskites $Gd_{0.2}Sr_{0.8}CoO_{3-\delta}$. The unit cells are shown by black lines. The O_2-site is a dominant position for oxygen vacancies at room temperature.

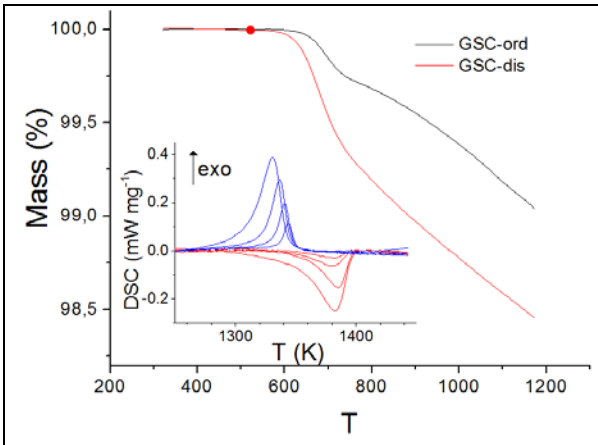

Figure 3: Thermogravimetric curves for samples $Gd_{0.2}Sr_{0.8}CoO_{3-\delta}$: black line for GSC-ord; red line for GSC-dis. 0.05% O_2-*Ar*, 0.166 K/s. The inset: DSC curves for heating (red) and cooling (blue) of $Gd_{0.2}Sr_{0.8}CoO_{3-\delta}$. 20% O_2-*Ar* mixture; cooling/heating ramp rates are 0.042, 0.083, 0.166 and 0.333 K/s.

The thermogravimetric (TG) curves for samples GSC-ord and GSC-dis are shown in Fig. 3. The samples under study were stable under argon atmosphere (0.05 % O_2) up to 550 K. At higher temperatures oxygen desorption occurred: the gradual mass decrease was accompanied by an increase of O_2^+ ion intensity (m/z = 32) in the mass-spectrum. It was noteworthy that the sample GSC-ord has lower oxygen content (higher index δ, Table 1) and smaller quantity of oxygen released during TG run (Fig. 3). To exclude the effect of the sample reduction on its physical properties at the first stage, the comparative analysis of sample properties has been restricted by a temperature range imposing constant oxygen content.

In Fig. 4 the linear thermal expansion coefficient α for the samples GSC-ord and GSC-dis are shown at heating up to T = 600 K. For the disordered sample GSC-dis in the temperature range 100 – 300 K we have found a wide minimum of $\alpha(T)$ at the temperature $T_{min\ GSC\text{-}dis} \approx 160$ K, that differs remarkably in shape and minima position from the similar data for the ordered sample GSC-ord with $T_{min\ GSC\text{-}ord} \approx 350$ K. The deformations $\Delta L/L$ (Fig. 4, insert) are also different.

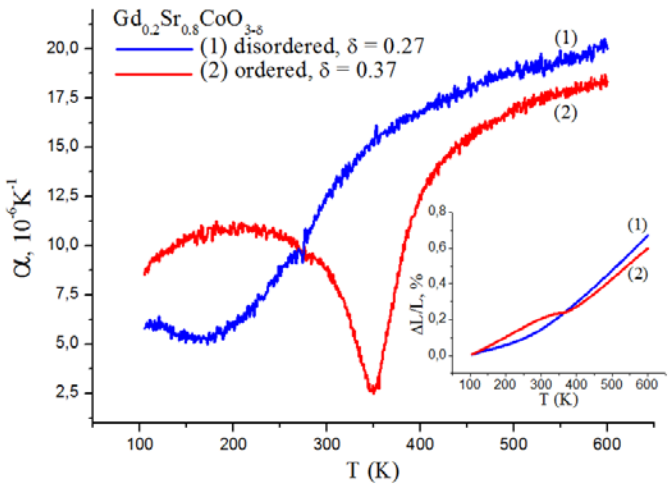

Figure 4: The temperature dependences of the linear thermal expansion coefficient for the samples $Gd_{0.2}Sr_{0.8}CoO_{3-\delta}$. The deformations $\Delta L/L$ are shown in the insert.

When heating up to 700 K the GSC-ord sample remains stable, the dependences $\alpha(T)$ and $\Delta L/L(T)$ do not change, while the behavior of the sample GSC-dis changes significantly. Fig. 5 gives the results of 5 heating cycles of the disordered sample up to 700 K and dilatation changes that we relate presumably to the increase of oxygen non-stoichiometry. It is evident from Fig. 5 that the minimum and its shape changes after the first heating to 700 K. At each next cycle of heating the minimum in $\alpha(T)$ becomes more pronounced and shifts to a higher temperature (Fig. 5 (b), insert), and tends to be more similar to the $\alpha(T)$ for the ordered sample GSC-ord. After the 5-th cycle the changes becomes insignificant, and $T_{min\ GSC\text{-}dis} < T_{min\ GSC\text{-}ord}$ always.

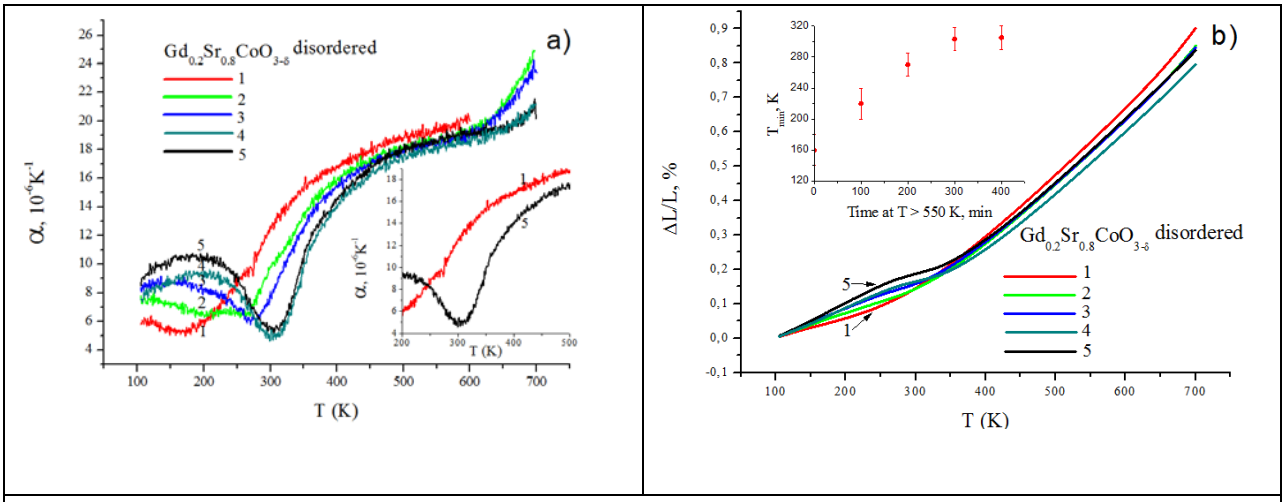

Figure 5: The temperature dependences of the linear thermal expansion coefficient *α* (a), and deformation *ΔL/L* (b), resulting from the consequent heating/cooling cycles (from first to fifth) for the disordered sample GSC-dis. The insert to (a) shows results of the first and fifth cycles. The insert to (b) shows the effect of the sample exposition at temperatures above 550 K on the *α(T)* minimum.

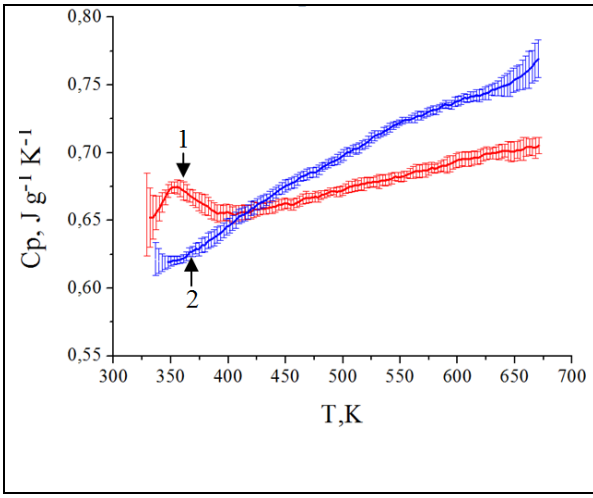

Figure 6: The temperature dependence of the specific heat capacity C_P (solid lines) and experimental error bars for GSC-ord (red) and GSC-dis (blue).

We have found that the temperature dependences of specific heat capacity C_P are significantly different for GSC-ord and GSC-dis samples. The $C_P(T)$ curve for the ordered sample GSC-ord has a pronounced maximum at 353 K (Fig. 6) corresponding to the minimum in the linear expansion coefficient. The C_P increase above 600 K in GSC-dis also correlates with the linear expansion data and may be related to the oxygen loss.

The temperature dependence of the magnetic susceptibility of the disordered sample GSC-dis measured in the zero field cooling (ZFC) and field cooling (FC) regimes in the field H = 1 kOe is shown in Fig. 7. At temperatures below 50 K and above 200 K the inverse susceptibility is linear and obeys the Curie-Weiss law (insert in Fig. 7) with the asymptotic Curie temperatures θ_C = -5.9 K and θ_C = 60 K respectively. The effective magnetic moment for low T (T < 50 K) and high T (T > 200 K) approximations are almost equal to each other. For the low T μ_{eff} = 4.69 ± 0.02 μ_B, and above 200 K it is equal to μ_{eff} = 4.61 ± 0.02 μ_B. Field dependences of magnetization at temperatures 300, 350, 400 K (Fig. 8) correspond to a paramagnetic behavior. From the field dependence of magnetization at T = 2 K (insert in Fig. 8) we can estimate the saturation value for the sample GSC-dis to be equal M_{sat} ≈ 1.38 μ_B/f.u.. This value is determines by the paramagnetic moment of Gd^{3+} ion (1/5 μ_{Gd} = 1/5×7μ_B = 1.4 μ_B).

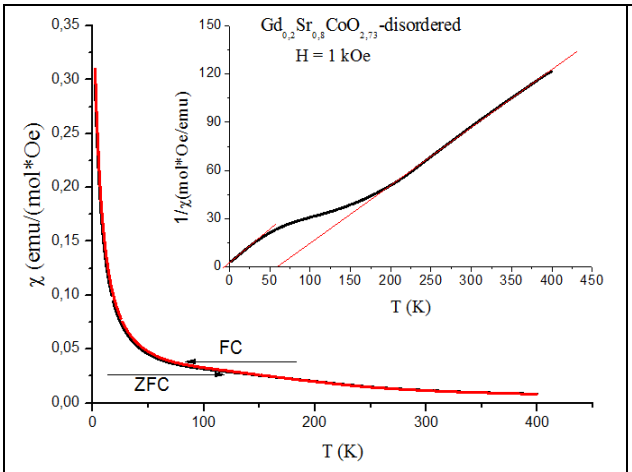

Figure 7: Temperature dependence of magnetic susceptibility for the GSC-dis sample measured in FC (black) and ZFC (red) modes in magnetic field H = 1 kOe. In the insert the inverse susceptibility vs temperature is shown with the Curie-Weiss

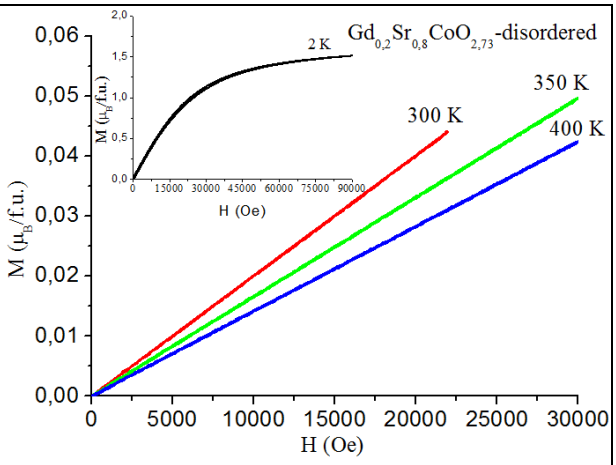

Figure 8: Magnetic field dependence of the GSC-dis sample magnetization at different temperatures. In the insert the magnetization curve at T = 2 K is shown.

approximation fitted by red lines.	

The temperature (Fig. 9) and field (Fig. 10, insert) dependences for the GSC-ord sample are similar to the disordered sample GSC-dis at low temperature. With increasing temperature we have found remarkable differences.

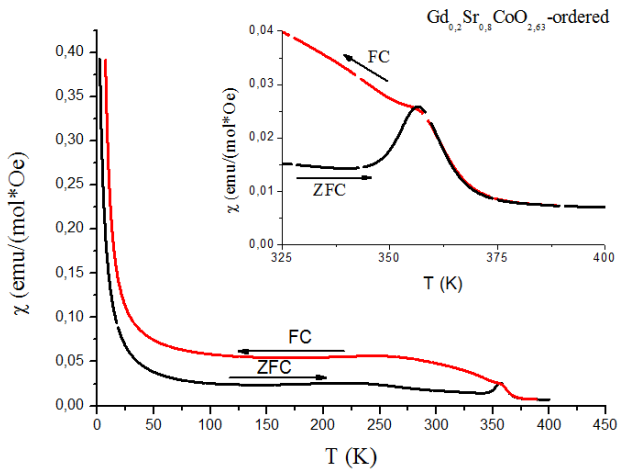

Figure 9: The temperature dependence of magnetic susceptibility for the GSC-ord sample measured in FC (red) and ZFC (black) modes in magnetic field H = 1 kOe. In the insert the susceptibility in the temperature range from 325 till 400 K is shown.

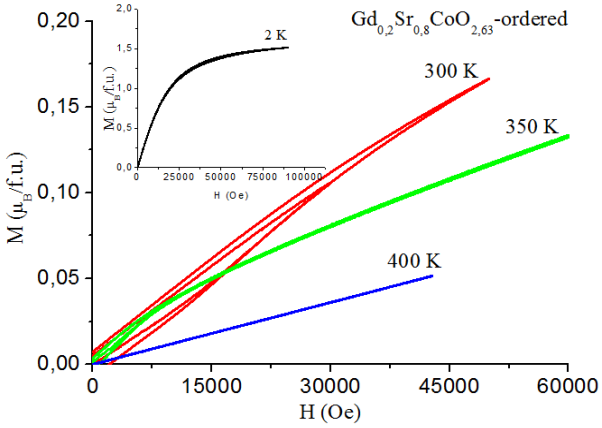

Figure 10: The magnetic field dependence of the GSC-ord sample magnetization at different temperatures. The magnetization curve at T = 2K (insert).

At the intermediate temperatures from 100 to 250 K a smooth increase of the magnetic susceptibility takes place. At higher temperatures the magnetic susceptibility decreases. At the temperature T_{max} = 355 K a magnetic anomaly with a sharp maximum in the magnetic susceptibility appears, indicating a transition to the paramagnetic state, with smaller magnetic susceptibility. A similar anomaly for the ordered phase of the $Gd_{0.5}Ba_{0.5}CoO_{2.9}$ with maximum of the magnetic susceptibility at 250 K has been found in.[41] The temperature T_{max} for the ordered

sample GSC-ord corresponds to the minimum in the linear thermal expansion coefficient $\alpha(T)$ and to the maximum in the molar heat capacity $C_P(T)$.

Thus we have found that at low temperatures in $GdCoO_3$[42] and $Gd_{0.2}Sr_{0.8}CoO_{3-\delta}$ the dominating magnetic interaction is the antiferromagnetic one that reveals itself against the background of the strong paramagnetism of the Gd^{+3} ions. When heating up to 350 K another magnetic state appears. Our static magnetization data do not allow to reveal the type of magnetic order in $Gd_{0.2}Sr_{0.8}CoO_{3-\delta}$ in the vicinity of the temperature T_{max}. The temperature and field dependence of the magnetization allows us to suggest presumably a cluster spin glass state rather than a ferromagnetic state. The susceptibility analysis in the FC and ZFC regimes (insert in Fig. 9) for the GSC-ord sample may be interpreted in terms of strong magnetic anisotropy in the ferromagnetic-like nanoclusters. In the ordered sample the difference of the ionic radii of the Gd^{+3} ions and Sr^{+2} ions results in local deformation, and in non-uniform magnetic separated state. As a result, there is a combination of anomalies of the thermodynamical properties, including the heat capacity and thermal expansion. Several mechanisms of magnetic state formation in *Sr/Ba* doped $GdCoO_3$ may be involved. Larger ionic radii of Sr^{+2} in comparison to the Gd^{+3} ion result in a local deformation that may change the relation between the crystal field value and the local Hund exchange interaction and induce a change of the spin state of the Co^{+3} ion from the low spin singlet to the intermediate S = 1 or high S = 2 state. Moreover, the ordered sample has larger deviations from the oxygen stoichiometry, with the ordered position of the oxygen vacancy. Regular absence of one oxygen ion results to the 5-coordinated pyramidal CoO_5-complex. In the crystal field of such coordination the Co^{+3} ion may be only in the high spin state.[43]

We also would like to discuss some similarities in the properties of doped cobaltates and relaxor ferroelectrics. The anomalies in the temperature dependence of the linear thermal expansion coefficient, the heat capacity, and the dielectric permeability at different frequencies

in relaxors[44-45] are quite similar to the anomalies in the temperature dependence of the linear thermal expansion coefficient, the heat capacity, and the magnetic susceptibility of our ordered doped cobaltates. From the phenomenological point of view, in relaxor ferroelectrics the electrostriction results in the correlation of electrical and dilatation properties. Similarly, in the ordered doped cobaltate $Gd_{0.2}Sr_{0.8}CoO_{3-\delta}$ the magnetostriction also may result in the correlation of the anomalies in the linear thermal expansion coefficient, the heat capacity, and the magnetization.

IV. Conclusion.

The thermoelectric figure of merit is determined in the following way: $ZT = (\sigma S^2 T/\varkappa)$, where σ is the electrical conductivity of a material, S is the Seebeck coefficient, $\varkappa$ is thermal conductivity, and T is the temperature. Thus, a good thermoelectric material should have simultaneously high electric conductivity, large Seebeck effect, and small thermal conductivity that is given by the sum of the electronic and lattice contributions $\varkappa = \varkappa_e + \varkappa_L$. To increase ZT the electronic conductivity should be as large as possible with the minimal heat conductivity. For good metals the Wiedemann-Franz law relates the electrical and heat conductivities: $\varkappa_e/\sigma = L_0 T$, where L_0 is the Lorenz parameter. So, optimization of the figure of merit ZT is not a simple task. The other important parameter for thermoelectrical applications is the factor of power $P = \sigma S^2$, it can be increased by doping the Mott insulators as we have done in substituted cobaltates with simultaneous decreasing of the heat conductivity. The decreasing of the lattice contribution $\varkappa_L$, that may be influenced by disorder, local deformations from the ionic radii and ionic masses mismatch, is another way to improve the material properties.

The rare-earth substituted cobaltates allow the possible realization of all suggested methods to increase the figure of merits. Moreover, cobaltates are the unic materials due to the proximity to the spin crossover. This proximity results in possible fluctuations of the *Co*

multiplicity that provides additional mechanism for phonon scattering processes. Large difference in the spin and orbital degeneration of the low and high spin *Co* states may also increase the thermoelectricity in cobaltates. One more peculiarity of cobaltates found in this paper is the large shift of the maximal rate of the phase transition from the cubic to the tetragonal phase depending on the cooling rate (Fig. 3, insert). Such behavior is typical for first order phase transitions and indicates the phase separation of a sample in the ordered and disordered regions, that may be of nanometer scale and have different crystal structure. Such phase separation may result in additional phonon scattering and improve the thermoelectric properties.

In summary, the interrelation of the anomalies in crystal lattice properties as the ionic order/disorder, thermal expansion, thermodynamical properties as heat capacity, and electronic/magnetic properties, such as magnetic susceptibility, found in this paper is important to evaluate the possibility of thermoelectric applications of these materials. Of course, the direct measurement of the transport and thermoelectric properties is required. It is outside the scope of present paper and will be a subject of the future study. The knowledge of the relation between order/disorder, oxygen vacancies with thermal treatment and properties provides a basis for reliable study of the transport properties.

Acknowledgments

Authors are thankful to Russian Science Foundation (project № 16-13-00060) for financial support. The magnetic measurements were carried out in the Shared Facility Centre of P. N. Lebedev Physical Institute of RAS

V. References

(1) Ivanova, N. B.; Ovchinnikov, S. G.; Korshunov, M. M.; Eremin, I. M.; Kazak, N. V. Specific Features of Spin, Charge, and Orbital Ordering in Cobaltates. *Phys. Usp.* **2009**, 52, 789-810.

(2) Knizek, K.; Jirak, Z.; Hejtmanek, J.; Veverka, M.; Marysko, M.; Maris, G.; Palstra, T. T. M. Structural Anomalies Associated with the Electronic and Spin Transitions in $LnCoO_3$. *Eur. Phys. J. B* **2005**, 47, 213-220.

(3) Radaelli, P. G.; Cheong, S.-W. Structural Phenomena Associated with the Spin-State Transition in $LaCoO_3$. *Phys. Rev. B* **2002**, 66, 094408.

(4) Sunstrom, J. E.; Ramanujachary, K. V.; Greenblatt, M.; Croft, M. The Synthesis and Properties of the Chemically Oxidized Perovskite, $La_{1-x}Sr_xCoO_{3-\delta}$ ($0.5 < x < 0.9$). *J. Solid State Chem.* **1998**, 139, 388-397.

(5) Scherrer, B.; Harvey, A. S.; Tanasescu, S.; Teodorescu, F.; Botea, A.; Conder, K.; Grundy, A. N.; Martynczuk, J.; Gauckler, L. J. Correlation Between Electrical Properties and Thermodynamic Stability of $ACoO_{3-\delta}$ Perovskites (A = La, Pr, Nd, Sm,Gd). *Phys. Rev. B* **2011**, 84, 085113.

(6) Tachibana, M.; Yoshida, T.; Kawaji, H.; Atake, T.; Takayama-Muromachi, E. Evolution of Electronic States in $RCoO_3$ (R = rare earth): Heat Capacity Measurements. *Phys. Rev. B* **2008**, 77, 094402.

(7) Mastin, J.; Einarsrud, M.-A.; Grande, T. Structural and Thermal Properties of $La_{1-x}Sr_xCoO_{3-\delta}$ ($0=x=0.4$). *Chem. Mater.* **2006**, 18, 6047-6053.

(8) Yoshii, K.; Tsutsui, S.; Nakamura, A. Magnetic and Structural Properties of $Pr_{1-x}A_xCoO_3$ (A = Sr and Ba). *JMMM* **2001**, 226, 829-830.

(9) Kaustuv Manna; Debakanta Samal; Suja Elizabeth; Bhat, H. L.; Anil Kumar, P. S. On the Magnetic Ground State of $La_{0.85}Sr_{0.15}CoO_3$ Single Crystals. *J. Phys. Chem. C* **2011**, 115, 13985-13990.

(10) Troyanchuk, I. O.; Bushinsky, M. V.; Sikolenko, V.; Efimov, V.; Ritter, C.; Hansen, T.; Tobbens, D. M. Pressure Induced Antiferromagnet-Ferromagnet Transition in $La_{0.5}Ba_{0.5}CoO_{2.8}$ Cobaltite. *Eur. Phys. J. B* **2013**, 86, 435.

(11) Karpinsky, D. V.; Troyanchuk, I. O.; Lobanovsky, L. S.; Chobot, A. N.; Ritter, C., Efimov, V.; Sikolenko, V.; Knolkin, A. L. Magnetic and Structural Phase Transitions in $La_{0.5}Sr_{0.5}CoO_{3-\delta}$ ($0 \leq \delta \leq 0.3$) Cobaltites. *J. Phys.: Condens. Matter* **2013**, 25, 316004.

(12) Goossens, D. J.; Wilson, K. F.; James, M.; Studer, A. J.; Wang, X. L. Structural and Magnetic Properties of $Y_{0.33}Sr_{0.67}CoO_{2.79}$. *Phys. Rev. B* **2004**, 69, 134411.

(13) Kobayashi, W.; Ishiwata, S.; Terasaki, I.; Takano, M.; Grigoraviciute, I.; Yamauchi, H.; Karppinen, M. Room-Temperature Ferromagnetism in $Sr_{1-x}Y_xCoO_{3-\delta}$ ($0.2 < x < 0.25$). *Phys. Rev. B* **2005**, 72, 104408.

(14) Brinks, H. W.; Fjellvag, H.; Kjekshus, A.; Hauback, B. C. Structure and Magnetism of $Pr_{1-x}Sr_xCoO_{3-\delta}$. *J. Solid State Chem.* **1999**, 147, 464-477.

(15) Haggerty, R. P.; Seshadri, R. Oxygen Stoichiometry, Crystal Structure, and Magnetism of $La_{0.5}Sr_{0.5}CoO_{3-\delta}$. J. *Phys.: Condens. Matter* **2004**, 16, 6477-6484.

(16) Troyanchuk, I. O.; Chobot, A. N.; Nikitin, A. V.; Mantytskaya, O. S.; Lobanovskii, L. S.; Dobryanskii, V. M. Influence of the Oxygen Content on the Magnetic and Transport Properties of the $La_{0.45}Ba_{0.55}CoO_{3-\delta}$ Cobaltites. *Phys. Solid State* **2015**, 57, 2427-2430.

(17) Pietosa, J.; Wisniewski, A.; Puzniak, R.; Fita, I.; Wojcik, M.; Paszkowicz, W.; Minikayev, R.; Nowak, J.; Lathe, Ch.; Kolesnik, S.; et al. Pressure Effect on Magnetic and Structural Properties of $La_{1-x}Sr_xCoO_{3-\delta}$. *Phys. Rev. B* **2009**, 79, 214418.

(18) Chen, Yi-Ch.; Yashima, M; Ohta, T.; Ohoyama, K.; Yamamoto, S. Crystal Structure, Oxygen Deficiency, and Diffusion Path of Perovskite-Type Lanthanum Cobaltites $La_{0.4}Ba_{0.6}CoO_{3-\delta}$ and $La_{0.6}Sr_{0.4}CoO_{3-\delta}$. *J. Phys. Chem. C* **2012**, 116, 5246-5254.

(19) Kozlovskii, A. A.; Khirnyi, V. F.; Semenov, A. V.; Puzikov, V. M.; Deineka, T. G.; Gaiduk, O. V.; Chiang, Yu. N. Effect of Tolerance Factor and A-site Cations Disorder on Transport Properties of $A1_{1-x}A2_xCoO_{3-\delta}$ Perovskites (A1 = Ho, Er; A2 = Ca, Sr). *Functional Materials* **2009**, 16, 292-301.

(20) Balamurugan, S.; Yamaura, K.; Arai, M.; Takayama-Muromachi, E. Charge Transport and Ferromagnetic Critical Behavior of the Correlated 3d Perovskite $Sr_{1-x}Ce_xCoO_3$. *Phys. Rev. B* **2007**, 76, 014414.

(21) Ovchinnikov, S. G.; Orlov, Yu. S., Dudnikov, V. A.; Vereshchagin, S. N.; Perov, N. S. Concentration Dependence of the Spin Gap in Solid Solutions $La_{1-x}Gd_xCoO_{3-\delta}$. *JMMM* **2015**, 383, 162-165.

(22) Vereshchagin, S. N.; Solovyev, L. A.; Rabchevskii, E. V.; Dudnikov, V. A.; Ovchinnikov, S. G.; Anshits, A. G. New Method for Regulating the Activity of ABO_3 Perovskite Catalysts. *Kinetics and Catalysis.* **2015**, 56, 640-645.

(23) Vereshchagin, S. N.; Solovyov, L. A.; Rabchevskii, E. V.; Dudnikov, V. A.; Ovchinnikov, S. G.; Anshits, A. G. Methane Oxidation Over A-site Ordered and Disordered $Sr_{0.8}Gd_{0.2}CoO_{3-\delta}$ perovskites. *Chem. Commun.* **2014**, 50, 6112 (5pp).

(24) Hashimoto, H.; Kusunose, T.; Sekino, T. Effects of Strontium Ion Doping on the Thermoelectric Properties of Dysprosium Cobalt Oxide. *Mater. Trans.* **2010**, 51, 404-407.

(25) Vulchev, V.; Vassilev, L.; Harizanova, S.; Khristov, M.; Zhecheva, E.; Stoyanova, R. Improving of the Thermoelectric Efficiency of $LaCoO_3$ by Double Substitution with Nickel and Iron. *J. Phys. Chem. C* **2012**, *116* (25), 13507-13515.

(26) Funahashi, R.; Matsubara, I.; Ikuta, H.; Takeuchi, T.; Mizutani, U.; Sodeoka, S. An Oxide Single Crystal with High Thermoelectric Performance in Air. *Jpn. J. Appl. Phys.* **2000**, 39, L1127-L1129.

(27) Funahashi, R.; Shikano, M. $Bi_2Sr_2Co_2O_y$ Whiskers with High Thermoelectric Figure of Merit. *Appl. Phys. Lett.* **2002**, 81, 1459-1461.

(28) Koumoto, K.; Terasaki, I.; Funahashi, R. Complex Oxide Materials for Potential Thermoelectric Applications. *Mater. Res. Bull.* **2006**, 31, 206-210.

(29) Baran, J. D.; Molinari, M.; Kulwongwit, N.; Azough, F.; Freer, R.; Kepaptsoglou, D.; Ramasse, Q. M.; Parker, S. C. Tuning Thermoelectric Properties of Misfit Layered Cobaltites by Chemically Induced Strain. *J. Phys. Chem. C* **2015**, *119* (38), 21818-21827.

(30) Tsuyoshi Takami *Functional Cobalt Oxides*; Pan Stanford Publishing Pte. Ltd., 2014.

(31) Bernard Raveau and Md. MotinSeikh *Cobalt Oxides*; published by Wiley-VCH, 2012.

(32) Wang, Y.; Fan, H. J. Improved Thermoelectric Properties of $La_{1-x}Sr_xCoO_3$ Nanowires. *J. Phys. Chem. C* **2010**, 114, 13947-13953.

(33) Visser, J. W. A Fully Automatic Program for Finding the Unit Cell from Powder Data. *J. Appl. Crystallogr.* **1969**, 2, 89-95.

(34) Rietveld, H. M. A Profile Refinement Method for Nuclear and Magnetic Structures. *J. Appl. Crystallogr.* **1969**, 2, 65-71.

(35) Solovyov, L. A. Full-Profile Refinement by Derivative Difference Minimization. *J. Appl. Crystallogr.* **2004**, 37, 743-749.

(36) Conder, K.; Pomjakushina, E.; Soldatov A.; Mitberg, E. Oxygen Content Determination in Perovskite-Type Cobaltates. *Mater. Res. Bull.* **2005**, 40, 257-263.

(37) James, M.; Cassidy, D.; Goossens, D. J.; Withers, R. L. The Phase Diagram and Tetragonal Superstructures of the Rare Earth Cobaltate Phases $Ln_{1-x}Sr_xCoO_{3-\delta}$ (Ln = La, Pr, Nd, Sm, Gd, Y, Ho, Dy, Er, Tm and Yb). *J. Solid State Chem.* **2004**, 177, 1886-1895.

(38) Withers, R. L.; James, M.; Goossens, D. J. Atomic Ordering in the Doped Rare Earth Cobaltates $Ln_{0.33}Sr_{0.67}CoO_{3-\delta}$ (Ln = Y, Ho and Dy). *J. Solid State Chem.* **2003**, 174, 198-208.

(39) James, M.; Tedesco, T.; Cassidy, D. J.; Withers, R. L. Oxygen Vacancy Ordering in Strontium-Doped Rare Earth Cobaltate Perovskites, $Ln_{1-x}Sr_xCoO_{3-\delta}$ (Ln = La, Pr and Nd; x > 0.60). *Mater. Res. Bull.* **2005**, 40, 990-1000.

(40) James, M.; Morales, L.; Wallwork, K.; Avdeev, M.; Withers, R.; Goossens, D. Structure and Magnetism in Rare Eath Strontium-Doped Cobaltates. *Physica B* **2006**, 385–386, 199-201.

(41) Kundu, A. K.; Sampathkumaran, E.V.; Rao, C. N. R. The Unusual Magnetic and Electronic Properties of $Gd_{0.5}Ba_{0.5}CoO_{2.9}$. *J. Phys. Chem. Solids* **2004**, 65, 95-100.

(42) Dudnikov, V. A.; Velikanov, D. A.; Kazak, N. V.; Michel, C. R.; Bartolome, J.; Arauzo, A.; Ovchinnikov, S. G.; Patrin, G. S. Antiferromagnetic Ordering in REM Cobaltite $GdCoO_3$. *Phys. Solid State* **2012**, 54, 79-83.

(43) Hu, Z.; Hua Wu; Haverkort, M. W.; Hsieh, H. H.; Lin, H.-J.; Lorenz, T.; Baier, J.; Reichl, A.; Bonn, I.; Felser, C.; et al. Different Look at the Spin State of Co^{3+} Ions in a CoO_5 Pyramidal Coordination. *Phys. Rev. Letters* **2004**, 92, 207402.

(44) Gorev, M. V.; Flerov, I. N.; Bondarev, V. S.; Sciau, Ph. Heat Capacity Study of Relaxor $PbMg_{1/3}Nb_{2/3}O_3$ in a Wide Temperature Range. *JETP* **2003**, 96, 531-537.

(45) Gorev, M. V.; Flerov, I. N.; Bondarev, V. S.; Maglione, M.; Simon, A. Thermal Expansion and Permittivity of $(Ba_{1-x}Bi_{2x/3})TiO_3$ Solid Solutions. *Phys. Solid State* **2011**, 53, 2073-2079.

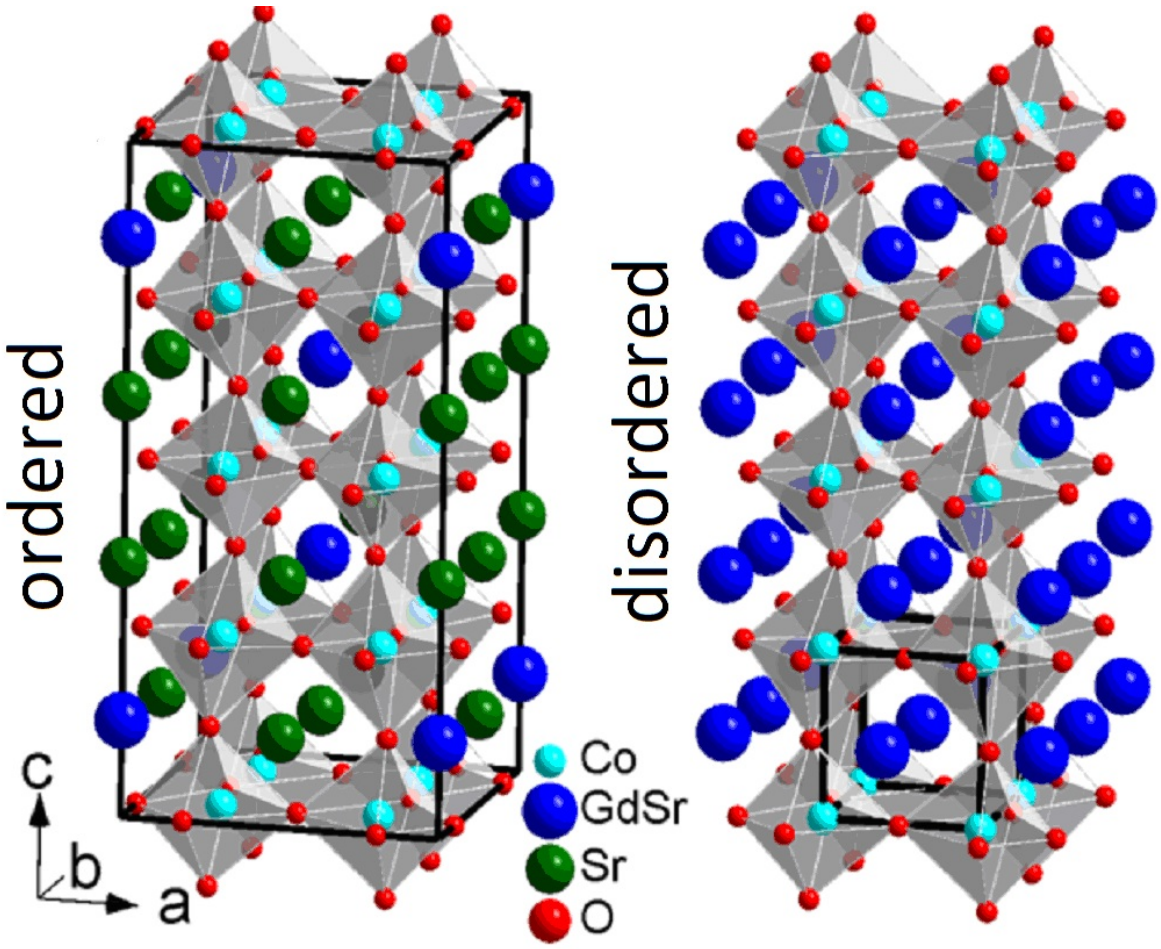

TOC: The ordered and disordered states of *Gd* and *Sr* in the *A*-sites of the crystal lattice of perovskite $Gd_{0.2}Sr_{0.8}CoO_{3-\delta}$.

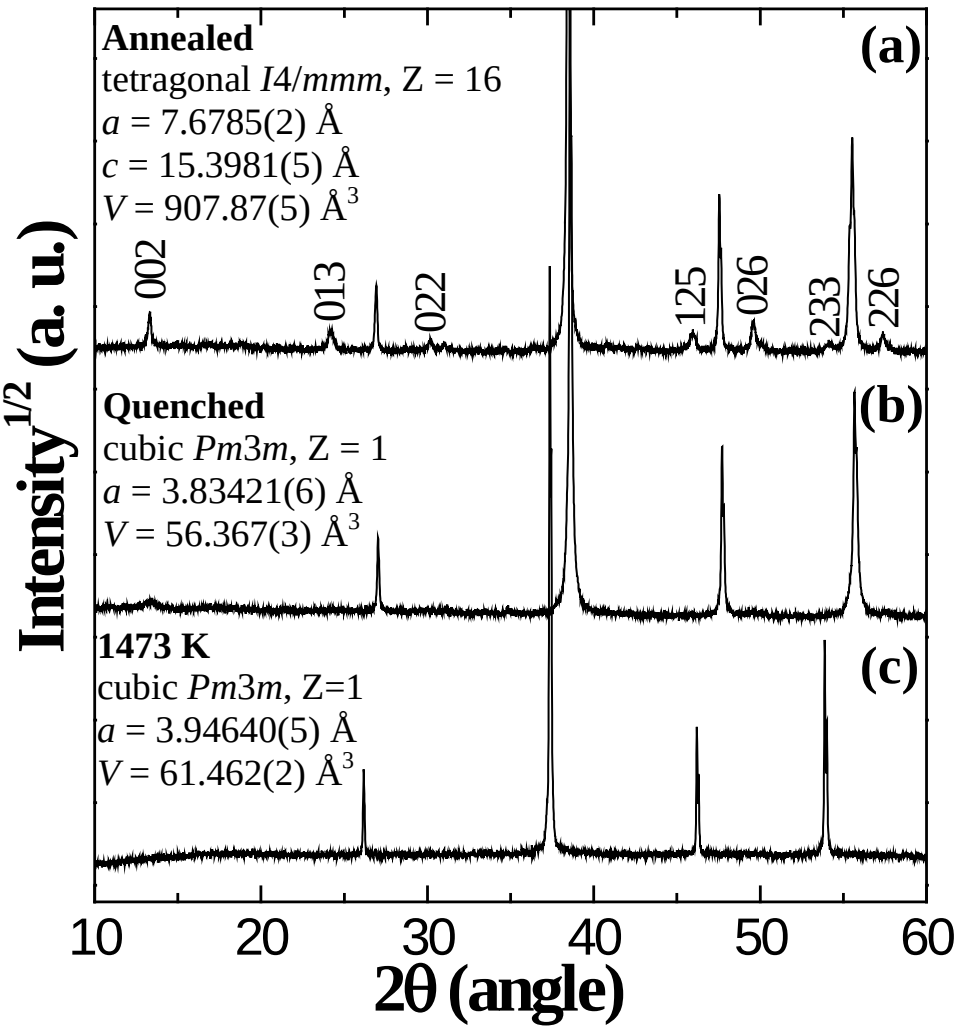

Fragments of XRD patterns of annealed sample GSC-ord (a), quenched sample GSC-dis (b), and sample at 1473 K (c). Tetragonal perovskite superstructure reflexions are indexed in (a). Lattice parameters and unit cell volumes are given in the inserts.

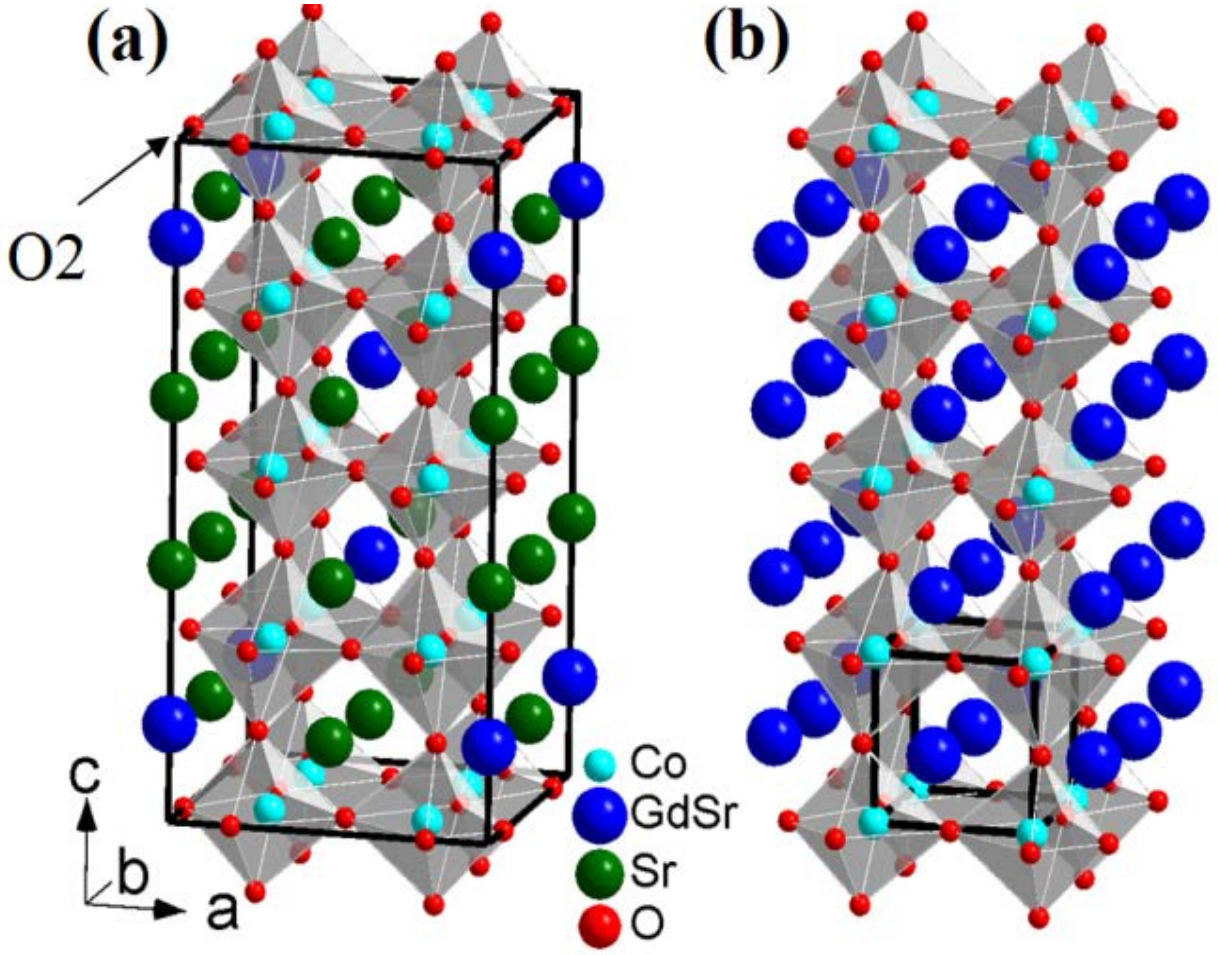

Crystal structures of the *A*-site ordered phase GSC-ord (a) and the disordered one GSC-dis (b) of perovskites $Gd_{0.2}Sr_{0.8}CoO_{3-\delta}$. The unit cells are shown by black lines. The O_2-site is a dominant position for oxygen vacancies at room temperature.

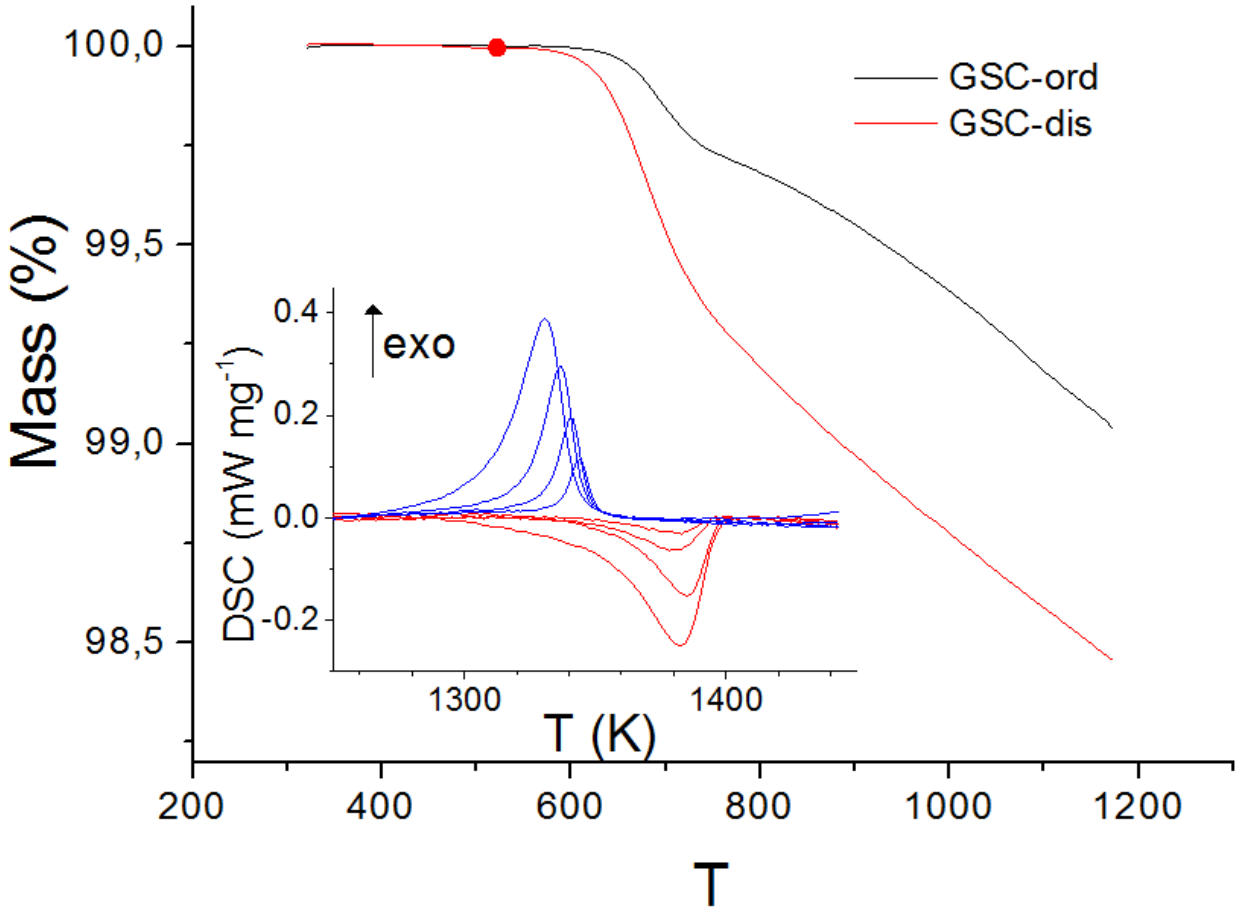

Thermogravimetric curves for samples $Gd_{0.2}Sr_{0.8}CoO_{3-\delta}$: black line for GSC-ord; red line for GSC-dis. 0.05% O_2-*Ar*, 0.166 K/s. The inset: DSC curves for heating (red) and cooling (blue) of $Gd_{0.2}Sr_{0.8}CoO_{3-\delta}$. 20% O_2-*Ar* mixture; cooling/heating ramp rates are 0.042, 0.083, 0.166 and 0.333 K/s.

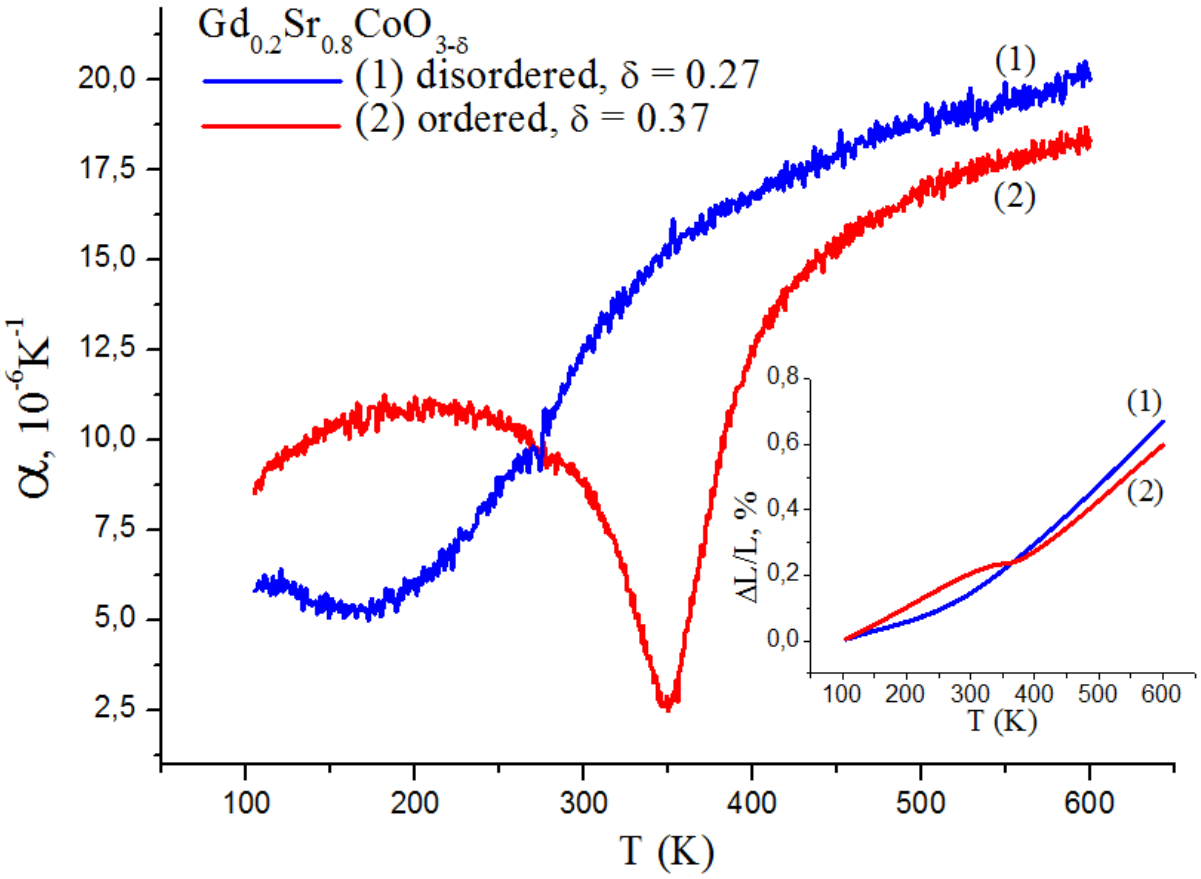

The temperature dependences of the linear thermal expansion coefficient for the samples $Gd_{0.2}Sr_{0.8}CoO_{3-\delta}$. The deformations $\Delta L/L$ are shown in the insert.

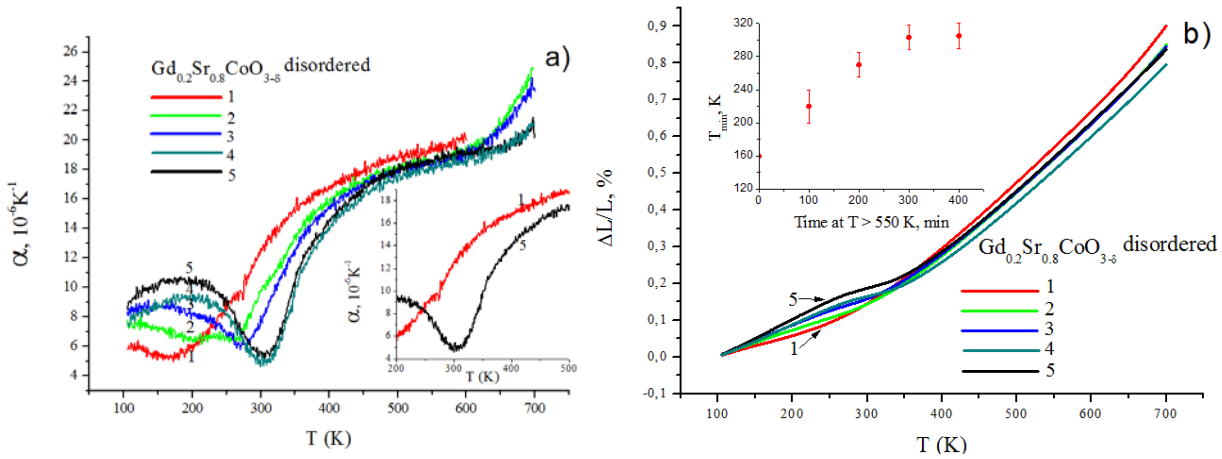

The temperature dependences of the linear thermal expansion coefficient *α* (a), and deformation *ΔL/L* (b), resulting from the consequent heating/cooling cycles (from first to fifth) for the disordered sample GSC-dis. The insert to (a) shows results of the first and fifth cycles. The insert to (b) shows the effect of the sample exposition at temperatures above 550 K on the *α(T)* minimum.

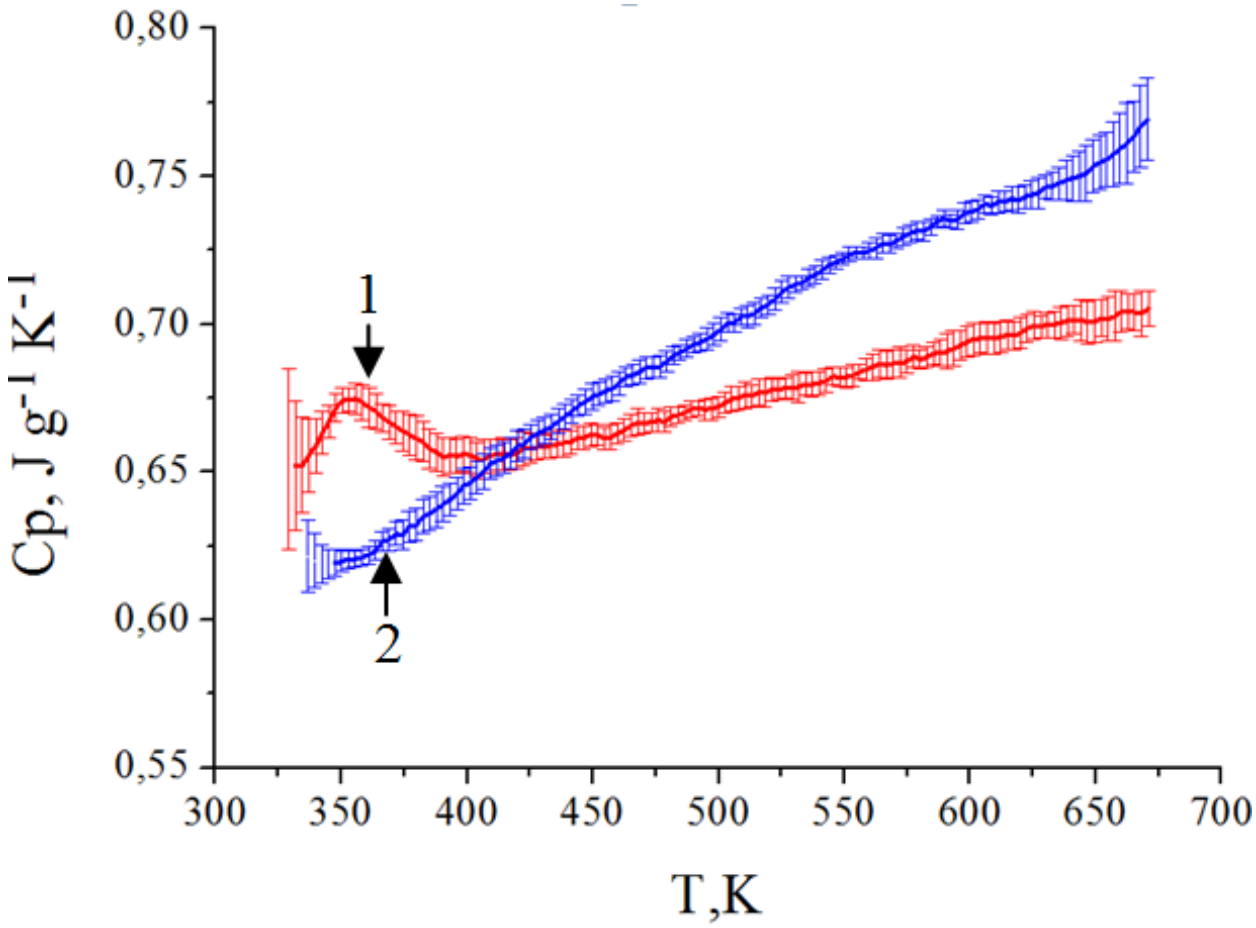

The temperature dependence of the specific heat capacity C_P (solid lines) and experimental error bars for GSC-ord (red) and GSC-dis (blue).

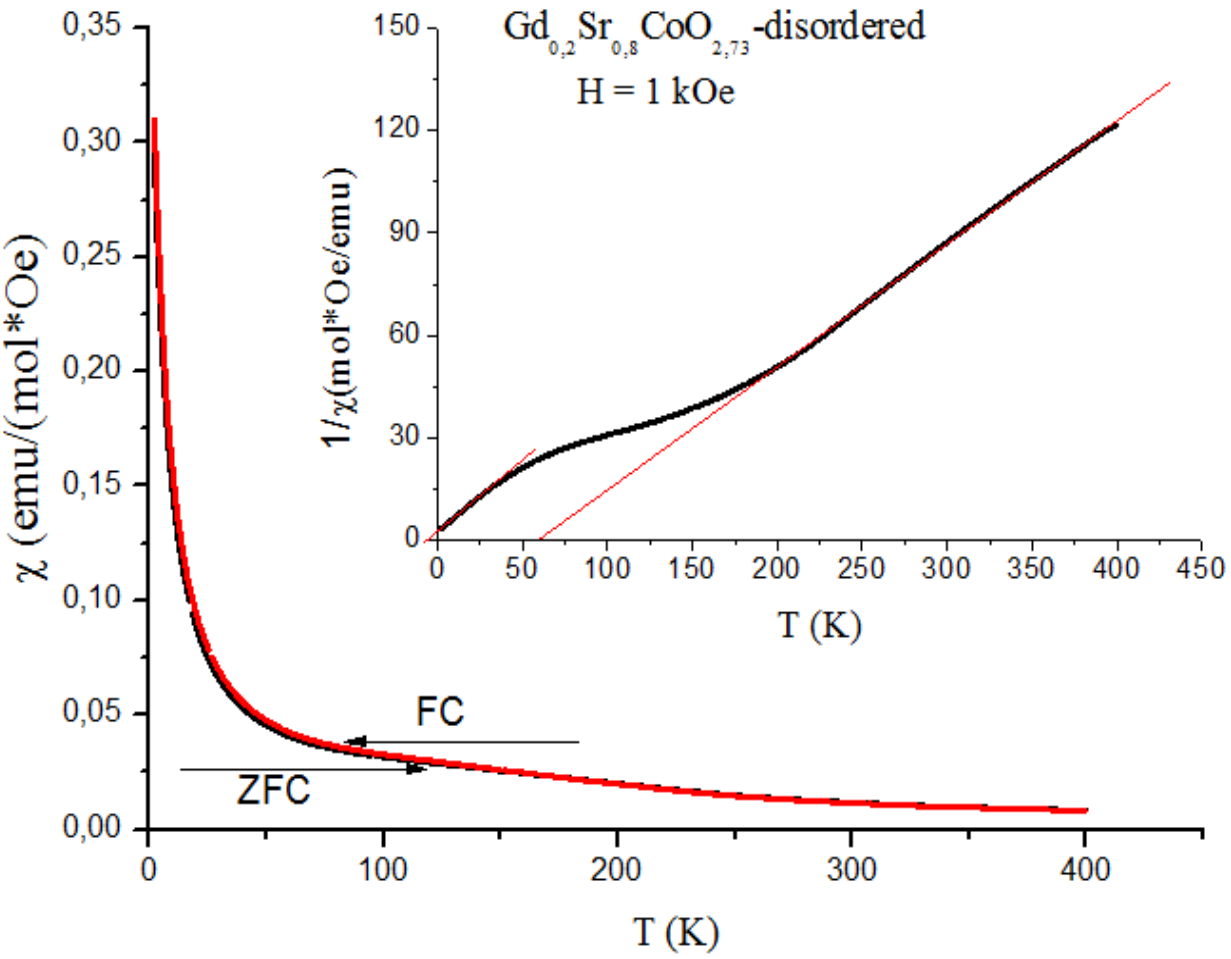

Temperature dependence of magnetic susceptibility for the GSC-dis sample measured in FC (black) and ZFC (red) modes in magnetic field *H* = 1 kOe. In the insert the inverse susceptibility vs temperature is shown with the Curie-Weiss approximation fitted by red lines.

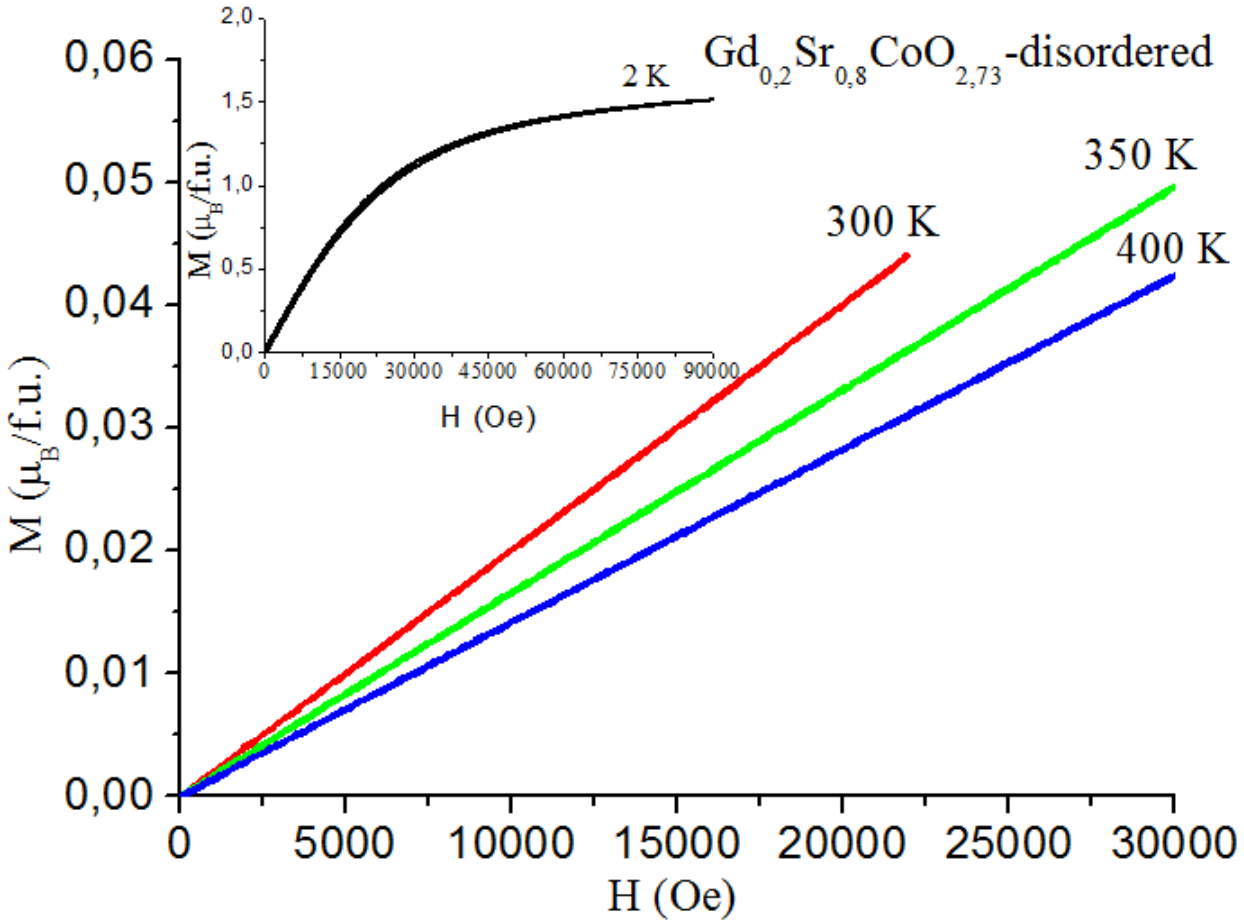

Magnetic field dependence of the GSC-dis sample magnetization at different temperatures. In the insert the magnetization curve at T = 2 K is shown.

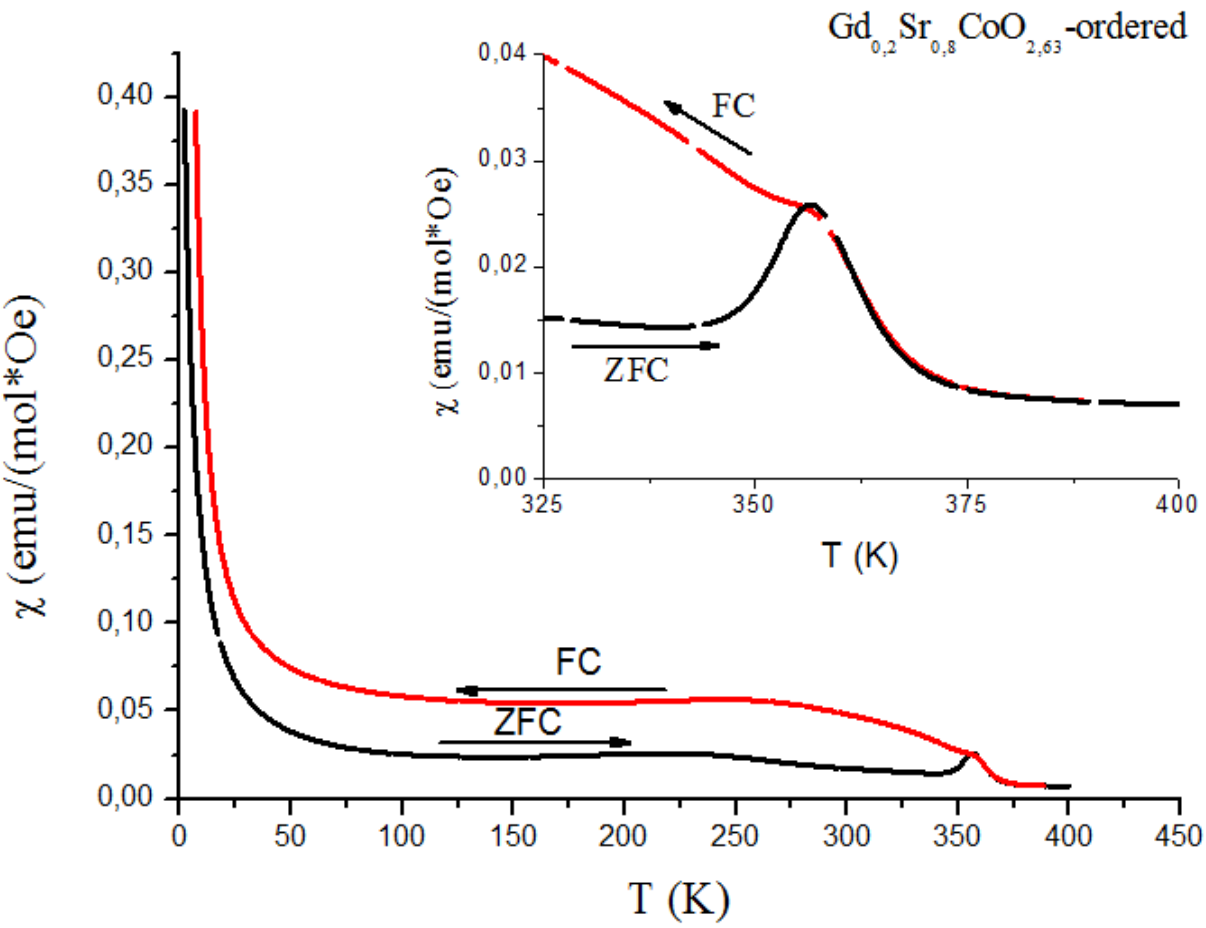

The temperature dependence of magnetic susceptibility for the GSC-ord sample measured in FC (red) and ZFC (black) modes in magnetic field *H* = 1 kOe. In the insert the susceptibility in the temperature range from 325 till 400 K is shown.

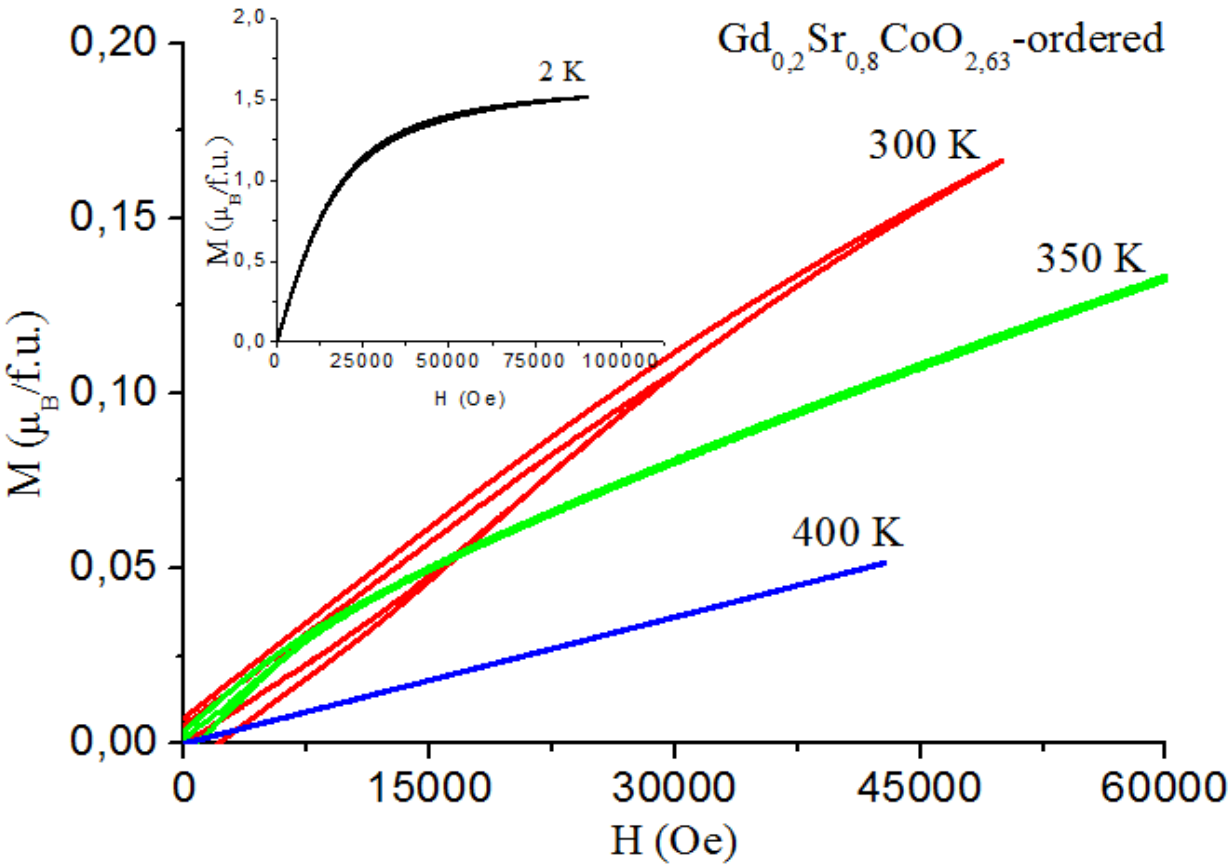

The magnetic field dependence of the GSC-ord sample magnetization at different temperatures. The magnetization curve at *T* = 2K (insert).